



# Dynamic mechanical properties and constitutive model of photosensitive resin specimens at different temperatures

Tao Liu<sup>1,2,3</sup> · Zhiqiang Yin<sup>1</sup> · Jingfa Lei<sup>1,2</sup> · Hong Sun<sup>1,2</sup> · Qiang Shen<sup>1</sup>

Received: 28 December 2022 / Accepted: 26 June 2023

Published online: 06 July 2023

© The Author(s) 2023

## Abstract

In order to reveal the dynamic mechanical properties of resin-molded parts prepared from photosensitive resin composition at different temperatures, four typical service temperatures (26 °C, 50 °C, 70 °C and 90 °C) were selected, and the mechanical properties of photosensitive resin specimens under quasi-static and high strain rate (1200 s<sup>-1</sup>, 1500 s<sup>-1</sup> and 1800 s<sup>-1</sup>) loading were tested by universal material testing machine and split Hopkinson pressure bar (SHPB) experimental device. The stress–strain data of the material were obtained. Results show that the stress of photosensitive resin specimens decreases with the increase of temperature under quasi-static and high strain rate loading conditions, reflecting a certain temperature softening effect. Two typical stages of strain softening and strain hardening exist in the quasi-static compression process of the specimens at room temperature, while the specimens only exhibit strain hardening at 50 °C, 70 °C and 90 °C. Under dynamic loading, the elastic modulus, peak stress and peak strain of the photosensitive resin increase with the increase of the strain rate, reflecting an obvious effect of strain rate strengthening. The nonlinear thermo-viscoelastic constitutive model can better describe the mechanical behavior of the material under high strain rates and service temperatures, and the experimental values are in good agreement with the fitted values of the model. The results can provide theoretical model and method support for the design and development of resin-based materials and the optimization of their mechanical properties.

**Keywords** Photosensitive resin · Dynamic mechanical properties · Temperature effect · Constitutive model

## 1 Introduction

Photosensitive resin usually refers to a type of resin material applied in the stereo lithography apparatus (SLA) process, whose liquid raw materials consist of monomers and prepolymers with the addition of photoinitiators. Under the irradiation of a certain wavelength of ultraviolet light, it will cause polymerization reaction and complete the liquid-to-solid conversion. Photosensitive resin products prepared by SLA process have the advantages of simple molding method, high material utilization rate and surface

quality, and are often used in industrial design, mold manufacturing, biomedicine [1] and so on. In these application scenarios, photosensitive resin components are often served in a wide temperature range and subjected to impact loading. Clarifying their dynamic mechanical properties and constructing a constitutive model that can accurately describe their mechanical behaviors are significant for the design and development of such materials, as well as the performance optimization of the components.

In the research of mechanical properties of photosensitive resin, universal testing machine and split

✉ Tao Liu, liutao19841015@163.com; tao.liu@ahjzu.edu.cn | <sup>1</sup>School of Mechanical and Electrical Engineering, Anhui Jianzhu University, 292 Ziyun Ave, Hefei 230601, Anhui, China. <sup>2</sup>Anhui Province Key Laboratory of Intelligent Manufacturing of Construction Machinery, Hefei 230601, Anhui, China. <sup>3</sup>Anhui Province Key Laboratory of Human Safety, Hefei 230601, Anhui, China.



Hopkinson bar device are often equipped to carry out experiments on the mechanical properties of materials under quasi-static and high strain rate loading. Through the rate-related mechanical property experiments of 3D printed polymer materials [2, 3], it is confirmed that these materials have significant strain rate effect. In addition, curing time and ambient temperature also affect the static and dynamic mechanical properties of photosensitive resin materials. With the increase of strain rate and curing time, the resin strength will increase accordingly [4]. For resin-based materials, the effects of temperature and strain rate on the mechanical properties of the materials were analyzed to further clarify that at low strain rate, the elastic modulus, yield stress and yield strain increased with the increase of strain rate and decreased with the increase of temperature. Under the same strain rate, the yield stress decreased with the increase of temperature [5]. In combination with the problem of rate-dependent large-deformation inelastic behavior, mechanical property tests over a wide strain rate range are carried out to simulate the high strain rate and temperature-dependent response of materials experiencing large-deformation inelastic strains under uniaxial compression [6].

Through material modification and structural optimization, the mechanical properties of photosensitive resin components can also be improved. In order to reveal the toughening mechanism of epoxy resin toughened by nano-rubber particles, the fracture toughness of the material was investigated at low ( $5 \times 10^{-4} \text{ s}^{-1}$ ,  $1 \times 10^{-1} \text{ s}^{-1}$ ,  $2.5 \times 10^{-1} \text{ s}^{-1}$ ) and high ( $90 \text{ s}^{-1}$ ) strain rates, and found that the toughening effect of nano-rubber particles on epoxy resin is significant at low strain rate while the toughening effect is significantly weakened at high strain rates [7]. In addition, quasi-static and dynamic compression experiments were used to reveal the effect of liquid nitrile butadiene rubber (LNBR) on the mechanical properties of epoxy resins [8], the effect of 2-Hydroxyethyl methacrylate-grafted graphene oxide (HEMA-g-GO) on the properties of photosensitive resins [9], and the effect of nanofibers on the mechanical properties of polymethyl methacrylate [10]. In order to understand the strengthening effect of structural improvement on the mechanical properties of the material, the additively-manufactured layered-hybrid lattice structure [11] and resin honeycomb structure [12, 13] were selected to carry out static and dynamic mechanical properties tests, and the strain distribution was analyzed by digital image correlation (DIC) method. It was pointed out that the root of rate dependent behavior is the inertia effect and inherent strain rate sensitivity of the material [11]. The material collapse strength and energy absorption properties are related to the delamination level of the honeycomb [12], and 3D

printed photosensitive resin structures have good vibration damping and deformation resistance [13].

In terms of test methods, SHPB (Split Hopkinson Pressure Bar) compression tests were performed on two types of resins (MMA-based resin and ABS-based tough resin) to infer their dynamic mechanical properties at high strain rates, and bar materials were optimized to improve test accuracy [14]. To fill the gap between quasi-static strain rates ( $< 10 \text{ s}^{-1}$ ) and high strain rates ( $> 1000 \text{ s}^{-1}$ ), the effect of medium strain rates on the tensile behavior of epoxy/clay nanocomposites was investigated [15].

Analysis of the current state of research reveals that with the rapid development of SLA technology, scholars and engineers have studied the effects of SLA processes, material modification and structural optimization on the mechanical properties of photosensitive resin after molding, and carried out the corresponding experimental technology research. However, there are few studies on the quasi-static and high strain rate mechanical properties of photosensitive resin specimens combined with the service temperature. The influence mechanism of service temperature (across glass transition temperature) on static and dynamic mechanical properties is still unclear, and the applicable constitutive model has not been constructed too.

In order to solve above problems, the photosensitive resin specimens prepared from photosensitive resin composition were selected, and the mechanical properties experiments were carried out under quasi-static ( $0.0008 \text{ s}^{-1}$ ) and high strain rate ( $1200 \text{ s}^{-1}$ ,  $1500 \text{ s}^{-1}$ ,  $1800 \text{ s}^{-1}$ ) loading at four service temperatures (room temperature,  $50 \text{ }^\circ\text{C}$ ,  $70 \text{ }^\circ\text{C}$ ,  $90 \text{ }^\circ\text{C}$ ). The effects of strain rate and ambient temperature on the dynamic mechanical properties of photosensitive resin materials were illustrated. Finally, a nonlinear thermo-viscoelastic constitutive model of photosensitive resin material is established by combining Mooney Rivlin model and Maxwell model. The established constitutive model can well describe the mechanical behavior of photosensitive resin under high strain rate and service temperature.

## 2 Experimental materials

The raw materials of photosensitive resin specimens for the experiments were provided by Beijing Daye 3D Technology Co., Ltd. The main components of the material were (meth)acrylate oligomers, (meth)acrylate monomers, photoinitiators and additives. Stereolithography apparatus (S130, Beijing Daye 3D Technology Co., Ltd.) was applied for the preparation of photosensitive resin specimens. The molding temperature of the specimens was  $26 \text{ }^\circ\text{C}$  and the layer thickness was  $0.1 \text{ mm}$ .

The schematic diagram of a typical SLA process is shown in Fig. 1. Firstly, a three-dimensional model of the specimen was established and converted into an STL (Stereo Lithography) format model, the model was imported into the equipment software, the model position is adjusted and supports are added. Then, the model is discretized and sliced to form two-dimensional data groups  $S_1, S_2, \dots, S_n$ . The laser and lifting platform are controlled according to the data group information. The first layer of curing is completed by reflecting the laser beam through the galvanometer and irradiating the liquid photosensitive resin to cure the irradiated area. Finally, the lifting platform is raised and the liquid resin is covered on the cured surface for the second layer of curing. In this way, the specimen preparation is completed through multi-layer curing.

The size of quasi-static specimen is determined to be  $\Phi 12 \text{ mm} \times 20 \text{ mm}$  according to GB/T1041-2008 [16]. Under the condition of high strain rate loading, the diameter of the specimen is set to be 12 mm according to the requirements of the SHPB experimental device, which did not exceed the diameter of the bar. In order to eliminate the inertia effect during the experiment, the specimen length is chosen to be 5 mm with the length-diameter ratio is 0.4167. The specimens is shown in Fig. 2.

The photosensitive resin specimen was tested in ATR (Attenuated Total Reflection) mode by Fourier infrared spectrometer (Nicolet 6700, Thermo Nicolet Corporation), with a measurement range of  $4000\text{--}500 \text{ cm}^{-1}$  and a resolution of  $4 \text{ cm}^{-1}$ . As shown in Fig. 3, the characteristic peak at  $1233 \text{ cm}^{-1}$  is attributed to the stretching vibrations of C–O–C bonds,  $1360 \text{ cm}^{-1}$  is attributed to the symmetric deformation vibration absorption peak of  $-\text{CH}_3$ , the strong peaks at  $1632$  and  $1718 \text{ cm}^{-1}$  are ascribed to the stretching vibrations of C=C and C=O bonds, respectively, and the characteristic peak at  $2860 \text{ cm}^{-1}$  is attributed to the stretching vibrations of C–H bonds in  $-\text{CH}_3$ . The above results indicated that the characteristic structural groups of the photosensitive resin have been successfully generated.

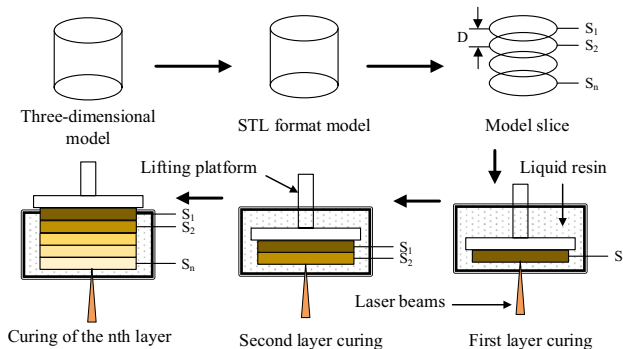


Fig. 1 Schematic diagram of SLA process

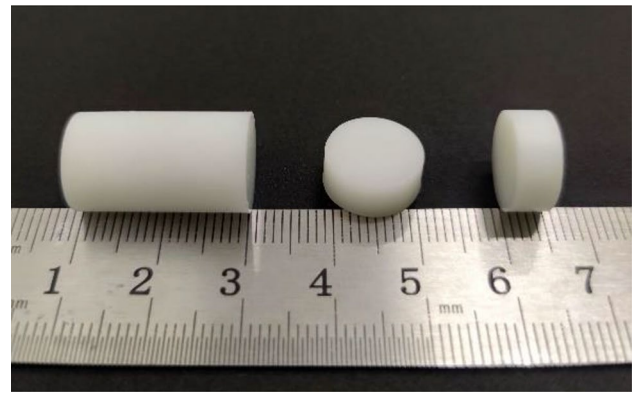


Fig. 2 Quasi-static and dynamic experimental specimens

The longitudinal and surface sampling of specimens were carried out, and the micro-morphology of the gold-sprayed specimens were observed by scanning electron microscope (Genimi SEM 500, Zeiss). As shown in Fig. 4a, after longitudinal large-area scanning, it's found that a uniform and orderly laminated structure is formed between the cured layers of the specimen, indicating that a relatively dense structure is formed during SLA process. Figure 4b shows the micro-morphology of the specimen surface. In the figure, the curing system presents an irregular bulk cross-linked structure, which is due to the chain polymerization reaction caused by free radical polymerization in SLA process. The molecular weight of the system is increased through polymerization, thus forming a cross-linked network.

A CT scanning system (CT-portable, Semi Material Technology (Beijing) Co., Ltd.) was used to scan the specimen,

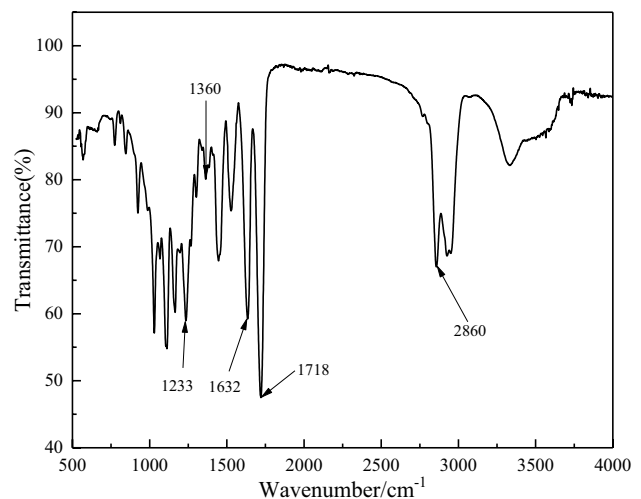
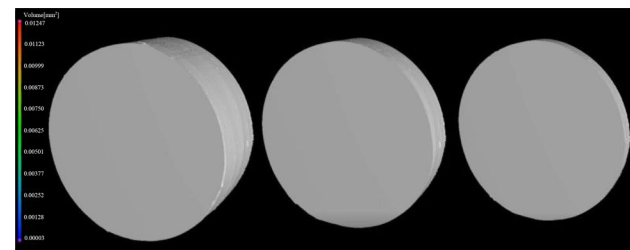
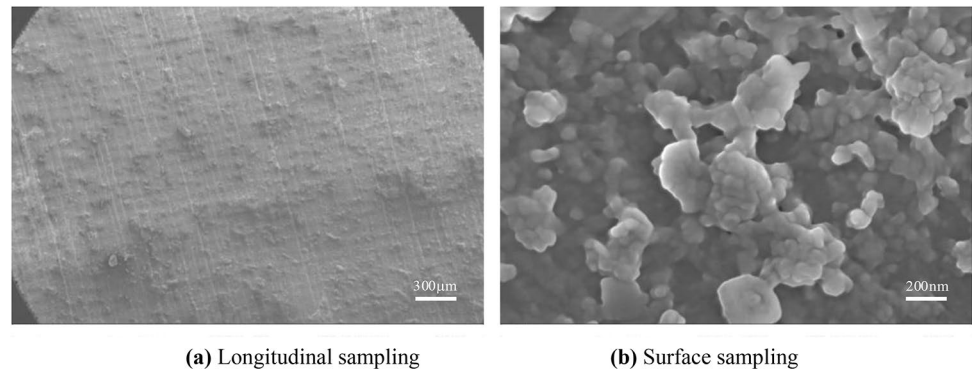


Fig. 3 FTIR (Fourier Transform Infrared Spectrometer) spectrum of the photosensitive resin specimen

**Fig. 4** Longitudinal and surface SEM pictures of the specimen



**Fig. 5** CT scan cross-sections of specimen

with an accelerating voltage of 30 kV, a current of 500 mA, an exposure time of 60 s, a number of shots of 1200, and a shooting time of 45 min. Figure 5 shows the CT scanning cross-sections of the specimen. It is found that the specimen can be penetrated, and no defects above 40 microns are found inside the specimen.

### 3 Quasi-static compression experiments

#### 3.1 Experimental device and method

A universal material testing machine (WDW-300A, Jinan Fangyuan Experimental Instrument Co., Ltd.) equipped with a temperature control device is used to carry out quasi-static compression experiments on photosensitive resin specimens. Four temperature conditions are selected, namely room temperature (26 °C), 50 °C, 70 °C, and 90 °C, with a loading speed of 1 mm/min and a loading strain rate of  $0.0008 \text{ s}^{-1}$ . The maximum strain of the specimens during the experiment is 0.3. To avoid the interference of chance factors, every experiment was repeated three times for each temperature condition.

#### 3.2 Experiment results and analysis

The stress–strain curves of the specimens under four temperature conditions are shown in Fig. 6. The quasi-static compression process of the specimens at room

temperature is divided into two stages: elastic and plastic. In the elastic stage, as the strain increases, the degree of nonlinearity of the stress–strain curve gradually increases, reflecting the characteristics of viscoelasticity. The plastic stage of the specimen begins from the yield point, and the plastic stage is divided into two typical processes too: strain softening and strain hardening. Just after the yield point, the stress decreases with the increase of strain, i.e., strain softening, after which the stress increases with the increase of strain and the phenomenon of strain hardening occurs.

Compared to room temperature, the specimens show a significant decrease in flow stress at three temperature conditions, 50 °C, 70 °C and 90 °C, with no yielding stage. The stress–strain curves of the photosensitive resin specimens all show a concave upward nonlinear variation law, that is, the stress increases rapidly with the increase of strain, showing the phenomenon of strain hardening. At the same time, the specimen stress decreases with the increase of temperature, indicating the temperature softening effect of the photosensitive resin specimens under quasi-static conditions.

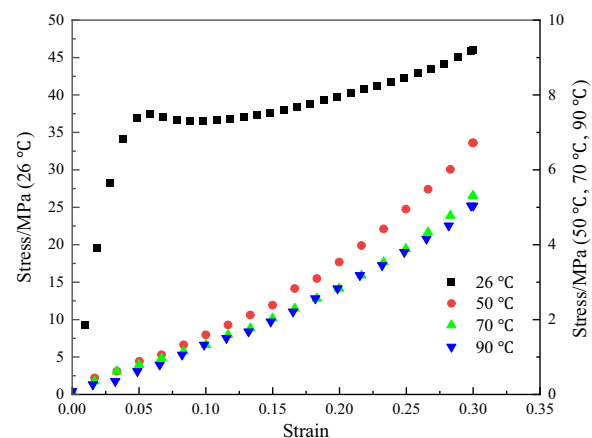


**Fig. 6** Quasi-static stress–strain curves of photosensitive resins with four temperatures



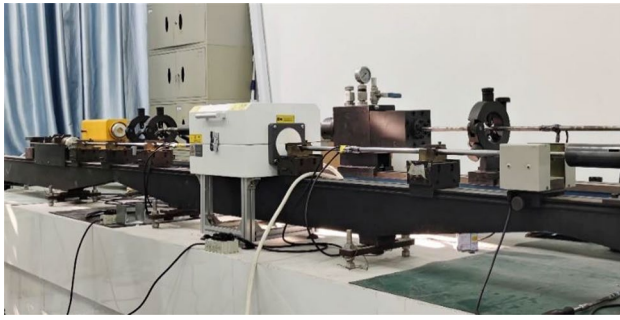


Fig. 7 Experimental system

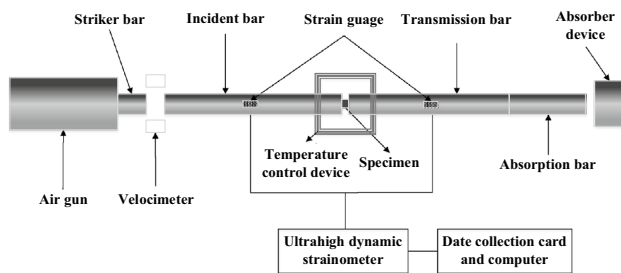


Fig. 8 Schematic diagram of the SHPB experimental device

## 4 Compression experiment at high strain rates

### 4.1 Experimental device and method

The dynamic (high strain rate) compression experiments were carried out using a split Hopkinson pressure bar (SHPB) experimental device equipped with a temperature control system (Fig. 7). Figure 8 is the schematic diagram of the SHPB device, in which the air gun is the launching device, and the bar system mainly consists of a striker bar (200 mm), an incident bar (1000 mm), a transmission bar (1000 mm) and an absorption bar (600 mm), all with diameter of 14.5 mm, material of 55CrSi spring steel, elastic modulus of 210 GPa, density of 7.85 g/cm<sup>3</sup> and wave velocity of about 5100 m/s. The test system consisted of strain gauges, an ultrahigh dynamic strainometer and a data acquisition system.

Two assumptions are required to conduct SHPB experiments, namely the one-dimensional stress wave assumption and the uniformity assumption [17]. In order to satisfy the assumption of one-dimensional stress wave, the length-to-diameter ratio of the incident and transmission bars was selected to be 68.97 (greater than 20), the length of the incident bar was 5 times that of the striker bar, the strain gauges were located in the middle of the bar, and the distance between the strain gauge and both ends of

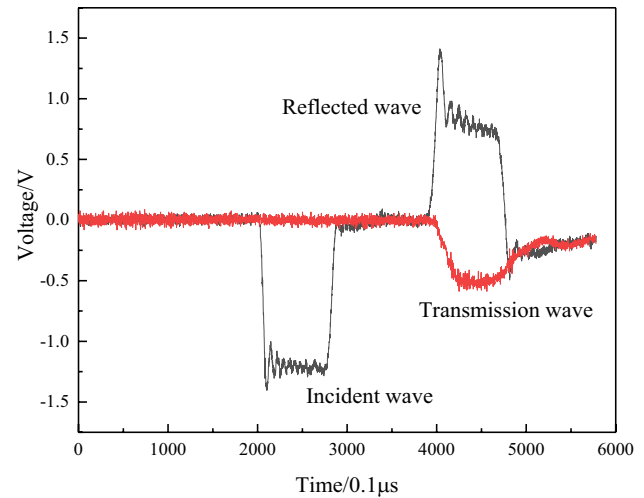


Fig. 9 Dynamic compression original waveform of photosensitive resin specimen

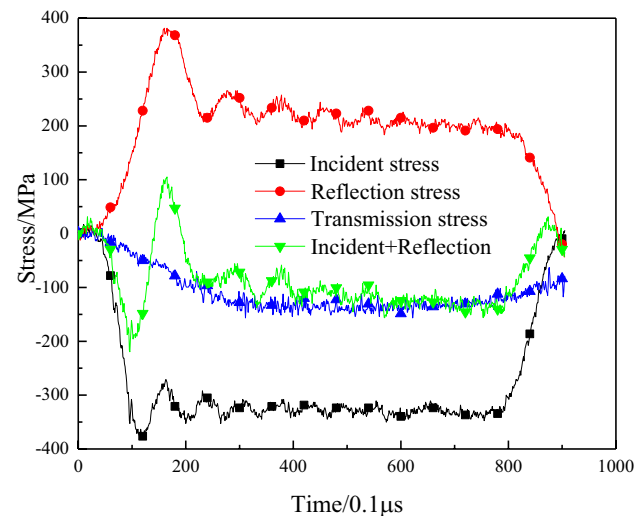


Fig. 10 Stress balance diagram of the specimen at a strain rate of 1500 s<sup>-1</sup>

the bar was greater than 10 times the bar diameter. During the experiment, the specimen was placed between the incident bar and the transmission bar, and the contact surface between the specimen and the bar was coated with lubricant (Vaseline) to reduce the friction effects [18]. Figure 9 shows the original waveform signals collected from the strain gauges under 1500 s<sup>-1</sup> strain rate loading at room temperature. Figure 10 shows the stress balance diagram of the specimen when the loading strain rate is 1500 s<sup>-1</sup>, in which the stress-time curve at the interface between the incident bar and the specimen was calculated by accumulating the incident and reflected signals, and the stress-time curve of the interface between the

transmission bar and the specimen was calculated from the transmission signal. It can be seen from the figure that the stress balance of the specimen is realized in the whole loading process, which conforms to the assumption of uniformity.

Figure 11 shows the high strain rate ( $1500 \text{ s}^{-1}$ ) loading process of the specimen at room temperature recorded by a high-speed camera (Phantom v1212, Vision Research Inc.). The process can be divided into four stages, the first frame before the deformation of the specimen corresponds to the first stage, when the specimen is in its original state and the striker bar hits the incident bar at a certain speed under the action of the air gun, and the incident bar generates an incident wave and an elastic strain  $\varepsilon_i$ ;  $0\text{--}17 \mu\text{s}$  is the second stage, the incident wave is transmitted to the specimen along the incident bar, and the specimen is deformed. Part of the incident wave is bounced back to form the reflected wave. The incident bar generates elastic strain  $\varepsilon_r$  again, and the other part is transmitted through the specimen to the transmission bar to form the transmitted wave and generate elastic strain  $\varepsilon_t$ . The third stage is at  $85 \mu\text{s}$ , when the maximum strain appears in the specimen and the stress wave pulse passes through the specimen completely; The fourth stage is right after  $85 \mu\text{s}$ , when the specimen thickness begins to recover, and the first loading ends.

In order to investigate the mechanical properties of materials under high strain rate loading, during the experiment, the impact velocity of the striker bar is changed by adjusting the air pressure of the launcher to achieve different strain rate loading. The relationship between the average engineering strain rate, the average engineering strain and the stress can be calculated by combining with the one-dimensional stress wave theory [19].

## 4.2 Experiment results and analysis

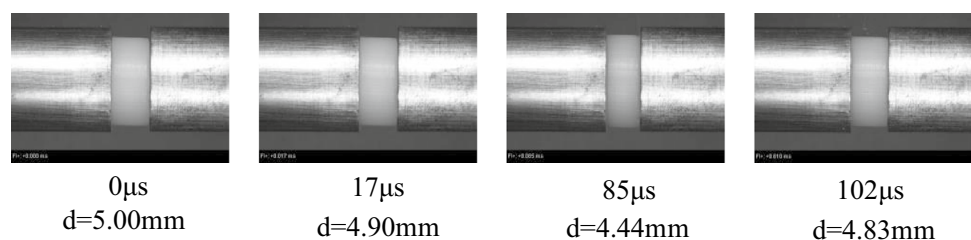
The dynamic compression experimental data of the photosensitive resin specimens were processed to obtain the stress–strain curves of the materials at the same temperature with different strain rates (Fig. 12) and the stress–strain curves of the materials at the same strain rate with different temperatures (Fig. 13).

It can be seen from Fig. 12 that the material has three typical stages of elasticity, plasticity and unloading under the action of dynamic compressive loading. It is generally considered that the elastic stage is before the yield point, in which the nonlinearity of the stress–strain curve gradually increases with the increase of the strain, and the material demonstrates the same viscoelastic characteristics as that under quasi-static loading. After reaching the yield limit, the material enters the plastic stage, where the stress decreases slowly with the increase of strain, reflecting the characteristics of strain softening, and the stress–strain curve of the material decreases sharply in the unloading stage.

Figure 13 shows the secant modulus (the slope of the line between the coordinate point and the origin when the strain of the stress–strain curve is 0.05), peak stress and peak strain data of each curve in Fig. 12. As shown in Fig. 13, the secant modulus, peak stress and peak strain increase with the increase of strain rate at four temperatures. As the strain rate increased from  $1200 \text{ s}^{-1}$  to  $1800 \text{ s}^{-1}$ , the secant modulus of the four temperature materials increased by 13%, 26%, and 17%, while the peak strain increased by 54%, 39%, and 44%, respectively. It shows that the photosensitive resin material has a significant strain rate effect. In order to compare the strain rate sensitivity of photosensitive resin under quasi-static and high strain rates, the slope of the yield stress–strain rate logarithmic curve of the material is defined as the strain rate sensitivity coefficient. The larger the slope the higher the strain rate sensitivity, and the relationship between the yield stress and strain rate of photosensitive resin at  $26 \text{ }^\circ\text{C}$  is shown in the Fig. 14, which shows that the strain rate sensitivity of the material at high strain rates is higher than that of low strain rates.

Combined with Figs. 13 and 15, it can be seen that the yield stress of the photosensitive resin material decreases with the increase of temperature at the same strain rate. In addition, the secant modulus of the specimen also decreases significantly with the increase of temperature. Obviously, the photosensitive resin materials also demonstrate temperature softening effects under high strain rates. The above temperature softening phenomenon is related to the change of mechanical state of the material when it crosses the glass transition

**Fig. 11** Loading process of the specimen at high strain rate ( $1500 \text{ s}^{-1}$ )



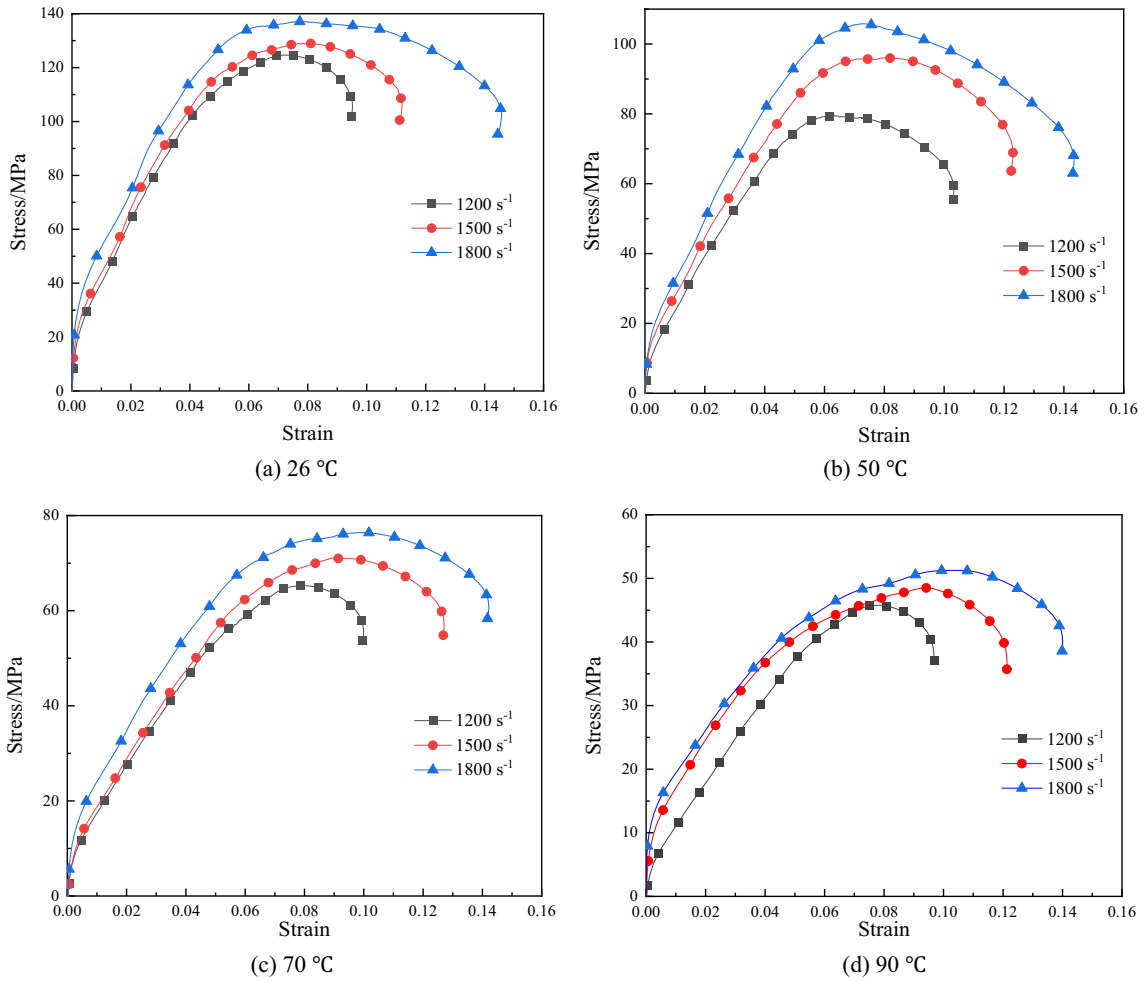


Fig. 12 Stress–strain curves of photosensitive resin at the same temperature with different strain rates

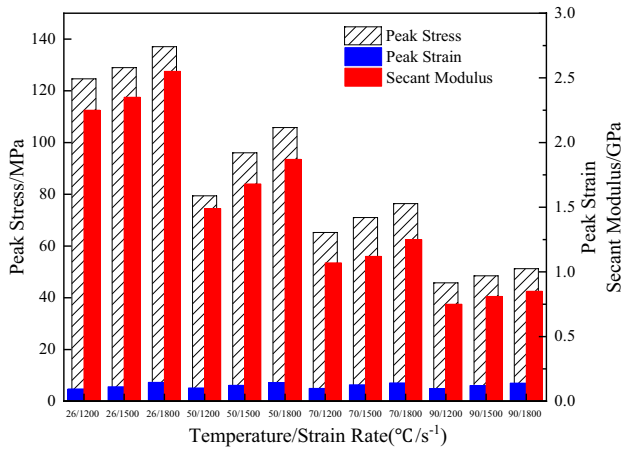


Fig. 13 Secant modulus, peak stress and peak strain at high strain rate and different temperatures

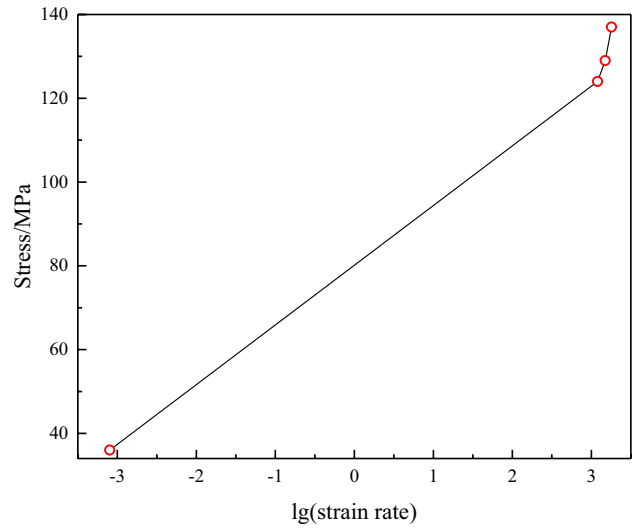


Fig. 14 Yield stress–strain rate logarithm curves

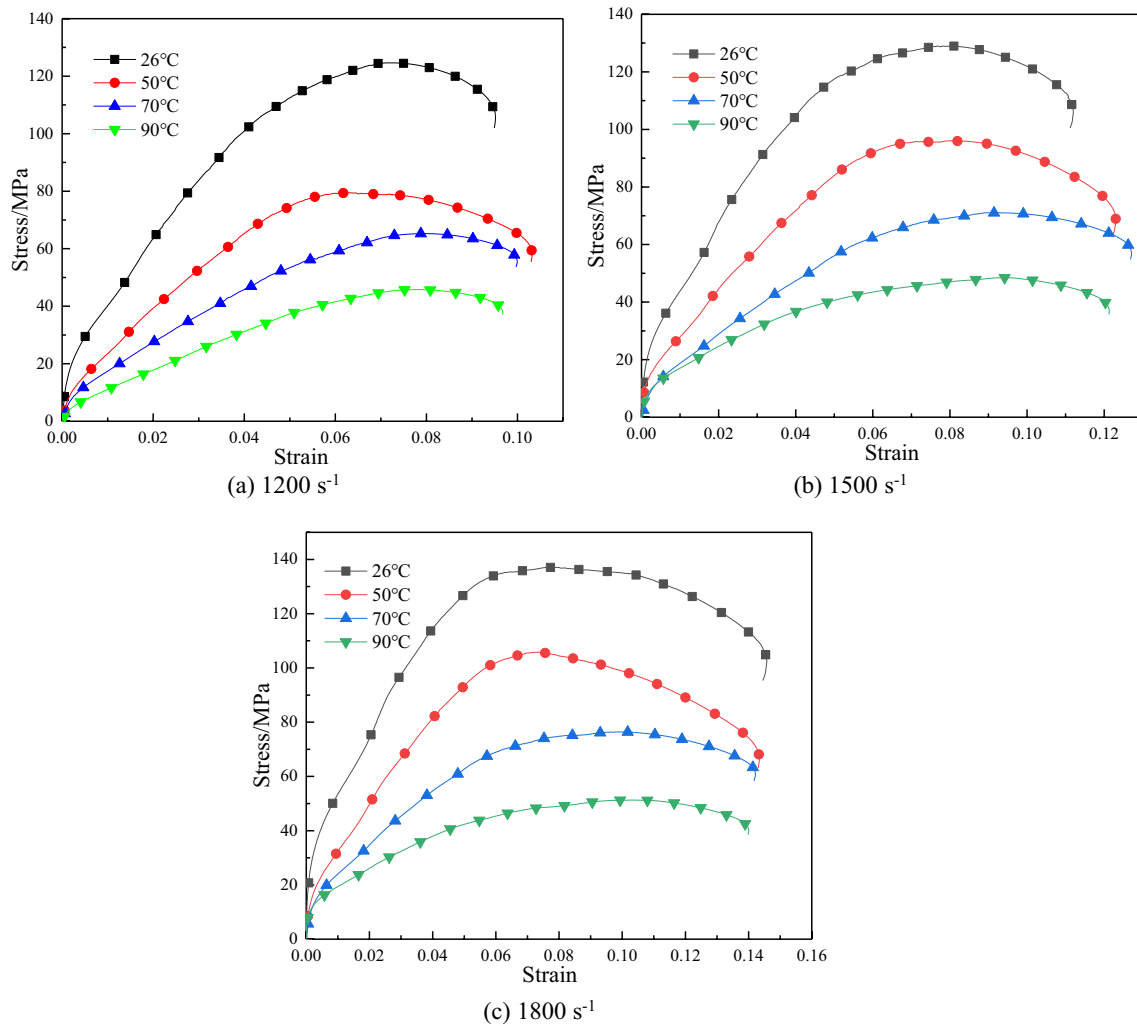


Fig. 15 Stress–strain curves for photosensitive resin at the same strain rate with different temperatures

temperature. As the temperature increases, the photosensitive resin changes from the glassy state to the rubbery state, and the corresponding molecular chain segments change from the frozen state to the thawed state, i.e., the macromolecular chains exhibit relaxation behavior. The strain rate strengthening effect of materials can be described from the perspective of microscopic molecular segment motion. As the strain rate increases, it becomes more difficult for the molecular chain segments to respond to external loads in time, and the chain segment movement is inactive. In terms of mechanical behavior expression, the above phenomenon is similar to the frozen state of chain segments at lower temperatures.

### 5 Nonlinear thermo-viscoelastic constitutive model

Through dynamic compression test, it is found that the mechanical behavior of photosensitive resin at different temperatures under high strain rate has nonlinear characteristics, which can be described by the hyperelastic model (Mooney–Rivlin model) [20]. At the same time, due to its temperature sensitivity, the material gradually loses its elastic characteristics under high temperature conditions and tends to be viscous fluidized, therefore, the Maxwell model [21] is introduced to express the viscoelastic properties of the photosensitive resin. In order to effectively describe the nonlinear mechanical behavior of photosensitive resin specimens at different



temperature under high strain rates, the Mooney–Rivlin model combined with the Maxwell model [22] is applied to establish the nonlinear thermo-viscoelastic constitutive model for photosensitive resin materials.

Assuming that the material is incompressible, the third invariant of the strain tensor in the hyperelastic constitutive equation is a constant value  $I_3 = 1$ , and the tensor expression of the material constitutive relation is:

$$\sigma^e = -p^e \mathbf{I} + 2 \left( \frac{\partial U}{\partial I_1} + \frac{\partial U}{\partial I_2} I_1 \right) \mathbf{B} - 2 \frac{\partial U}{\partial I_2} \mathbf{B} * \mathbf{B} \quad (1)$$

where,  $\sigma^e$  is the Cauchy stress tensor (or true stress tensor),  $p^e$  is the hydrostatic pressure,  $\mathbf{I}$  is the unit tensor,  $\mathbf{B}$  is the left Cauchy-Green deformation tensor,  $I_1, I_2$  are the first and second invariants of tensor  $\mathbf{B}$  respectively,  $U = U(I_1, I_2)$  is the strain energy function of unit volume [23].

Under uniaxial compression,  $\sigma_{11}^e = \sigma_{true}^e, \sigma_{22}^e = \sigma_{33}^e = 0$ , the constitutive equation for the uniaxial compression stress state is shown in Eq. (3),

$$\begin{cases} \sigma_{11}^e = -p^e + 2 \left( \frac{\partial U}{\partial I_1} + \frac{\partial U}{\partial I_2} I_1 \right) \mathbf{B}_{11} - 2 \frac{\partial U}{\partial I_2} \mathbf{B}_{11}^2 \\ \sigma_{22}^e = \sigma_{33}^e = -p^e + 2 \left( \frac{\partial U}{\partial I_1} + \frac{\partial U}{\partial I_2} I_1 \right) \mathbf{B}_{11}^{-1/2} - 2 \frac{\partial U}{\partial I_2} \mathbf{B}_{11}^{-1} = 0 \end{cases} \quad (2)$$

$$\sigma_{11}^e = \sigma_{True} = 2 \left( \lambda^2 - \frac{1}{\lambda} \right) \left( \frac{\partial U}{\partial I_1} + \frac{1}{\lambda} \frac{\partial U}{\partial I_2} \right) \quad (3)$$

The strain energy function is described by the Mooney–Rivlin constitutive model as follows:

$$U = A_1(I_1 - 3) + A_2(I_2 - 3) \quad (4)$$

Substituting Eq. (4) into Eq. (3), the hyperelastic response of the material is obtained as:

$$\sigma_{True} = 2(\lambda - \lambda^{-2})(A_1 \lambda + A_2) \quad (5)$$

where,  $A_1$  (MPa) and  $A_2$  (MPa) are material constants respectively,  $\lambda$  is the elongation.

Combining the M-R hyperelastic constitutive model with a single Maxwell element, the nonlinear viscoelastic constitutive model is obtained as shown in Eq. (6).

$$\sigma_{True} = 2(\lambda - \lambda^2)(A_1 \lambda + A_2) + E_3 \int_0^t \lambda \exp\left(-\frac{t-\tau}{\theta_3}\right) d\tau \quad (6)$$

Moreover, the nonlinear thermo-viscoelastic constitutive model is obtained by considering the parameters of the constitutive model as temperature-dependent quantities, as shown in Eq. (7),

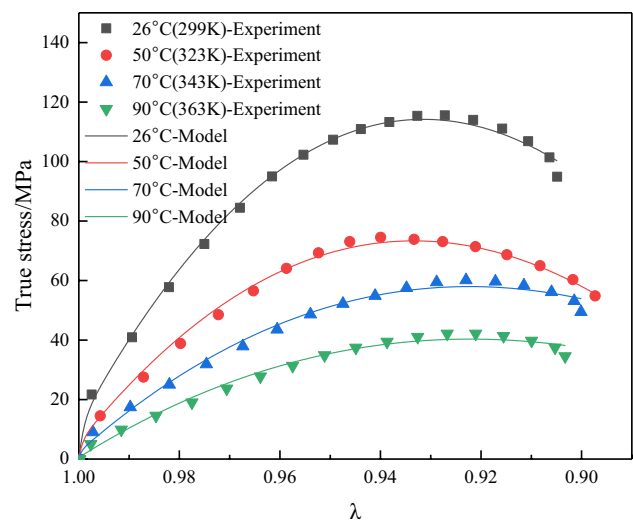


Fig. 16 Comparison between fitting curves and experimental data

Table 1 Fitting parameter values of M-R-Maxwell model

| Temperature | $A_1$ /MPa | $A_2$ /MPa | $E_3$ /MPa | $\theta_3$ /s | $R^2$ |
|-------------|------------|------------|------------|---------------|-------|
| 299 K       | 10,850     | - 9303     | 11,566     | 8.39E-7       | 0.996 |
| 323 K       | 7591       | - 6541     | 7935       | 5.89E-7       | 0.994 |
| 343 K       | 4571       | - 3828     | 4945       | 4.03E-7       | 0.991 |
| 363 K       | 3260       | - 2730     | 2684       | 1.70E-7       | 0.986 |

$$\sigma_{True} = 2(\lambda - \lambda^2)(A_1(T)\lambda + A_2(T)) + E_3(T) \int_0^t \lambda \exp\left(-\frac{t-\tau}{\theta_3(T)}\right) d\tau \quad (7)$$

In Eq. (7),  $T$  is the Kelvin temperature,  $A_1$  (MPa),  $A_2$  (MPa) and  $E_3$  (MPa) are the material constants and  $\theta_3$  (s) is the relaxation time.

The stress–strain curves of the photosensitive resin at  $1200 \text{ s}^{-1}$  strain rate and four temperatures are selected and calculated to be transformed into the true stress–elongation relationship curve and fitted by least squares. The results are shown in Fig. 16, and the fitted parameters are shown in Table 1. The model shows very good results for fitting highly nonlinear segments, this is due to the fact that the M-R-Maxwell model has fewer fitting parameters, and the fitting does not require restrictions on the fitting parameters, which increases the fitting flexibility. Due to the above advantages that the M-R-Maxwell model has similar fitting results at  $1500 \text{ s}^{-1}$  and  $1800 \text{ s}^{-1}$ .

From the regularity of each parameter value, it is easy to know that each parameter can be considered as a primary or quadratic function form of  $(T - T_0)$  (where the reference temperature  $T_0 = 299 \text{ K}$ ), and fitted by least squares, respectively, with the results shown in Fig. 17 and Table 2. The expressions of each temperature-related

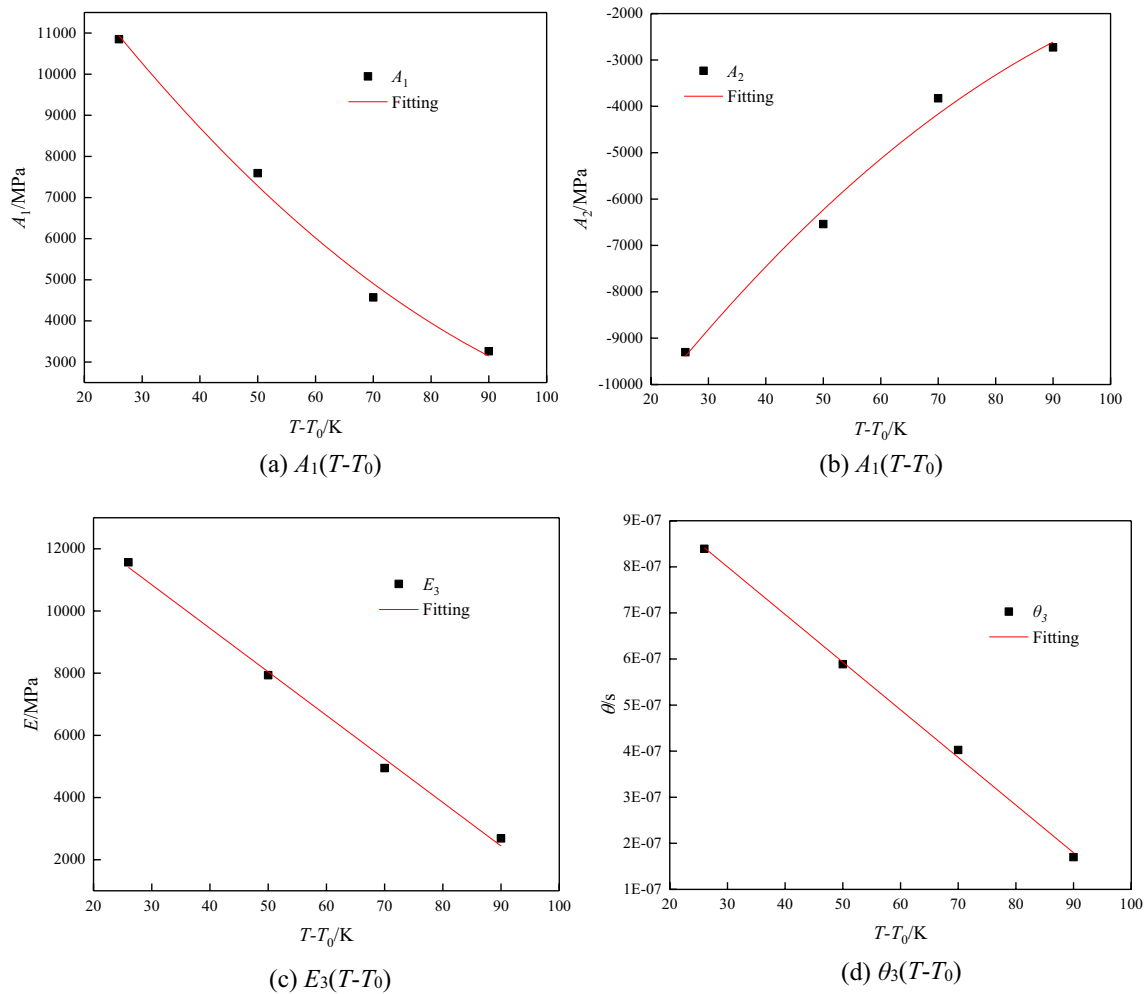


Fig. 17 Fitting relationship between parameters and temperature

parameter are shown in Eq. (8). By substituting Eq. (8) into Eq. (7), the thermo-viscoelastic constitutive model of photosensitive resin at a strain rate of  $1200 \text{ s}^{-1}$  considering temperature is obtained.

$$\begin{cases} A_1 = -210(T - 299) + 0.76(T - 299)^2 + 15890 \\ A_2 = 180(T - 299) - 0.64(T - 299)^2 - 13650 \\ E_3 = -140(T - 299) + 15047 \\ \theta_2 = -1.03 * 10^{-8} (T - 299) + 1.11 * 10^{-6} \end{cases} \quad (8)$$

Table 2 Fitting correlation coefficient of each parameter

|       | $A_1(T - T_0)/\text{MPa}$ | $A_2(T - T_0)/\text{MPa}$ | $E_3(T - T_0)/\text{MPa}$ | $\theta_3(T - T_0)/\text{s}$ |
|-------|---------------------------|---------------------------|---------------------------|------------------------------|
| $R^2$ | 0.993                     | 0.991                     | 0.996                     | 0.998                        |

## 6 Discussion

Through quasi-static and dynamic mechanical property experiments, the mechanical property data of photosensitive resin specimens at four different service temperature were obtained. Through the analysis of stress-strain curves, it is found that the material demonstrate temperature softening phenomenon under quasi-static and dynamic loading, which could be explained from the perspective of dislocation motion.

Under the action of dynamic loading, the dislocations between the molecular chains of the material overcome various microscopic energy barriers and produce macroscopic plastic distortions. The amplitude of atomic thermal vibration increases with the increase of temperature. The corresponding thermal energy facilitates dislocations crossing the short-range potential barriers, known as thermal activation. The thermal activation energy increases with the increase of temperature and decreases with the

increase of strain rate. The corresponding stress decreases with the increase of temperature and increases with the increase of strain rate, resulting in a strain rate effect. On the other hand, the temperature softening phenomenon of the material can also be described from the point of view of the physical state (mechanical state). Photosensitive resin material belongs to cross-linked polymer. When the temperature is low, the specimen is in the glassy state and the thermal motion of the chain segments is not sufficient to overcome the rotational barriers within the main chain, when the chain segments are in a frozen state. When the temperature rises to the glass transition temperature, the chain segments begin to thaw and the conformation of the macromolecular chain changes, exhibiting relaxation behavior. The temperature softening phenomenon of photosensitive resin can be attributed to the transition of these two mechanical states.

Furthermore, the analysis of the stress–strain curves also reveals that the strain rate effect and the temperature effect have similar effects on the mechanical properties of photosensitive resin material, and there is an equivalent relationship between rate and temperature, which shows that the effect of reducing ambient temperature is equivalent to that of increasing strain rate. However, the mechanical behavior of photosensitive resin materials under the combined effect of strain rate and temperature is very complex, such as whether there is a competition mechanism between actual heating and equivalent cooling (i.e., reducing strain rate). Clearly describing rate-temperature dependent dynamic distortion relationship with wide strain rates and wide temperature ranges is still a scientific problem to be solved.

## 7 Conclusion

A static and dynamic mechanical property test platform was built, and mechanical property experiments were carried out on photosensitive resin specimens with selected four service temperatures (26 °C, 50 °C, 70 °C, 90 °C) and four strain rates (0.0008 s<sup>-1</sup>, 1200 s<sup>-1</sup>, 1500 s<sup>-1</sup>, 1800 s<sup>-1</sup>). The conclusions are as follows:

(1) Under quasi-static loading, the stress of the photosensitive resin specimens decreases with the increase of temperature, which reflects a certain temperature softening effect. The quasi-static compression process at room temperature (26 °C) is divided into two stages: elastic and plastic, and the plastic stage is divided into two typical processes: strain softening and strain hardening. Under the three temperature conditions of 50 °C, 70 °C and 90 °C, the stress of the photosensitive resin specimens increase rapidly with

the increase of strain, showing the phenomenon of strain hardening.

- (2) Under high strain rate loading, the stress–strain curve of photosensitive resin has three typical stages: elasticity, plasticity and unloading. Under the four service temperatures, its elastic modulus, peak stress, and peak strain all increase with the increase of strain rate, reflecting the obvious strain rate strengthening effect. In addition, the material also demonstrates a temperature softening effect similar to quasi-static loading.
- (3) The mechanical properties of photosensitive resin at high strain rates have a rate-temperature equivalent relationship. The constructed nonlinear thermo-viscoelastic constitutive model of photosensitive resin materials can better describe the mechanical behavior of materials at high strain rates and service temperatures.

The conclusions of this study can provide references for the optimization of mechanical properties and impact resistance design of photosensitive resin materials. In order to clarify the correlation between the strain rate effect and temperature effect of photosensitive resin, it is necessary to expand the range of temperature and strain rate, and carry out research on rate-temperature equivalence and its correlation mechanism.

**Author contributions** TL: investigation, writing—original draft, writing—review and editing. ZY: formal analysis, investigation, methodology, writing—original draft. JL: investigation, conceptualization, resources, supervision. HS: conceptualization, project administration, investigation, validation, visualization. QS: conceptualization, formal analysis, investigation, methodology.

**Funding** This work was supported by the National Natural Science Foundation of China (No. 51805003), Anhui Education Department Excellent Young Talent Support Project (No. gxyqZD2019057), and the Foundation of Anhui Province Key Laboratory of Human Safety (No. DEPS-2021-02).

**Availability of data and material** The data used to support the findings of this study are available from the corresponding author upon request.

**Code availability** Not applicable.

## Declarations

**Conflict of interest** The authors declare that there is no conflict of interest regarding the publication of this paper.

**Ethical approval** Not applicable.

**Consent to participate** Written informed consent for publication was obtained from all participants.

**Consent for publication** Written informed consent for publication was obtained from all participants.

**Open Access** This article is licensed under a Creative Commons Attribution 4.0 International License, which permits use, sharing, adaptation, distribution and reproduction in any medium or format, as long as you give appropriate credit to the original author(s) and the source, provide a link to the Creative Commons licence, and indicate if changes were made. The images or other third party material in this article are included in the article's Creative Commons licence, unless indicated otherwise in a credit line to the material. If material is not included in the article's Creative Commons licence and your intended use is not permitted by statutory regulation or exceeds the permitted use, you will need to obtain permission directly from the copyright holder. To view a copy of this licence, visit <http://creativecommons.org/licenses/by/4.0/>.

## References

1. Baudis S, Heller C, Liska R, Stampfl J, Bergmeister H, Weigel G (2009) (Meth)Acrylate-based photoelastomers as tailored biomaterials for artificial vascular grafts. *J Polym Sci Pol Chem* 47(10):2664–2676. <https://doi.org/10.1002/pola.23352>
2. Wang YT, Li X, Chen Y, Zhang C (2021) Strain rate dependent mechanical properties of 3D printed polymer materials using the DLP technique. *Addit Manuf* 47:102368. <https://doi.org/10.1016/j.addma.2021.102368>
3. Miedzinska D, Gieleta R, Malek E (2020) Experimental study of strength properties of SLA resins under low and high strain rates. *Mech Mater* 141:103245. <https://doi.org/10.3390/ma13245825>
4. Miedzinska D, Gieleta R, Poplawski A (2020) Experimental study on influence of curing time on strength behavior of SLA-printed samples loaded with different strain rates. *Materials* 13(24):5825. <https://doi.org/10.3390/ma13245825>
5. Luo G, Wu CB, Xu KL, Liu LL, Chen W (2021) Development of dynamic constitutive model of epoxy resin considering temperature and strain rate effects using experimental methods. *Mech Mater* 159:103887. <https://doi.org/10.1016/j.mechmat.2021.103887>
6. Tamrakar S, Ganesh R, Sockalingam S, Haque BZ, Gillespie JW (2020) Strain rate-dependent large deformation inelastic behavior of an epoxy resin. *J Compos Mater* 54(1):71–87. <https://doi.org/10.1177/0021998319859054>
7. Xu F, Guo WG, Fu KK, Wang XJ (2015) Toughening mechanism of nano-rubber particles in epoxy resin under different strain rates. *Acta Polym Sin* 9:1092–1099. <https://doi.org/10.1177/j.issn1000-3304.2015.15022>
8. Xu X, Gao SQ, Ou ZC, Ye HF (2018) Mechanical behavior of liquid nitrile rubber-modified epoxy resin under static and dynamic loadings: experimental and constitutive analysis. *Materials* 11(9):1565. <https://doi.org/10.3390/ma11091565>
9. Li JH, Wang LF, Dai LJ, Zhong LP, Liu B, Ren JH, Xu YF (2018) Synthesis and characterization of reinforced acrylate photosensitive resin by 2-hydroxyethyl methacrylate-functionalized graphene nanosheets for 3D printing. *J Mater Sci* 53(3):1874–1886. <https://doi.org/10.1007/s10853-017-1432-8>
10. Goncalves NI, Munchow EA, Santos JD, Sato TP, de Oliveira LR, Paes TJD, Bottino MC, Borges ALS (2020) The role of polymeric nanofibers on the mechanical behavior of polymethyl methacrylate resin. *J Mech Behav Biomed* 112:104072. <https://doi.org/10.1016/j.jmbbm.2020.104072>
11. Li S, Hu ML, Xiao LJ, Song WD (2020) Compressive properties and collapse behavior of additively-manufactured layered-hybrid lattice structures under static and dynamic loadings. *Thin Wall Struct* 157:107153. <https://doi.org/10.1016/j.tws.2020.107153>
12. Hong H, Hu ML, Dai LS (2021) Dynamic mechanical behavior of hierarchical resin honeycomb by 3D printing. *Polymers* 13(1):19. <https://doi.org/10.3390/polym13010019>
13. Zhu DM, Ding F, Liu HP, Liu GY (2019) Mechanical properties of a photosensitive resin structure. *Chin J Eng* 41(4):512–520. <https://doi.org/10.13374/j.issn2095-9389.2019.04.012>
14. Aghayan S, Bieler S, Weinberg K (2021) Determination of the high-strain rate elastic modulus of printing resins using two different split Hopkinson pressure bars. *Mech Time-depend Mat* 26(4):761–773. <https://doi.org/10.1007/s11043-021-09511-2>
15. Gurusideswar S, Velmurugan R, Gupta NK (2016) High strain rate sensitivity of epoxy/clay nanocomposites using non-contact strain measurement. *Polymer* 86:197–207. <https://doi.org/10.1016/j.polymer.2015.12.054>
16. GB/T 1041-2008 (2008) Plastics—determination of compressive properties. Standards Press of China (in Chinese Beijing)
17. Zhu J, Hu SS, Wang LL (2009) An analysis of stress uniformity for concrete-like specimens during SHPB tests. *Int J Impact Eng* 36(1):61–72. <https://doi.org/10.1016/j.ijimpeng.2008.04.007>
18. Lu FY, Lin YL, Wang XY, Lu L, Chen R (2015) A theoretical analysis about the influence of interfacial friction in SHPB tests. *Int J Impact Eng* 79:95–101. <https://doi.org/10.1016/j.ijimpeng.2014.10.008>
19. Wang LL, Wang YG (2005) The important role of stress waves in the study on dynamic constitutive behavior of materials by SHPB. *Explos Shock Waves* 25(01):17–25. [https://doi.org/10.11883/1001-1455\(2005\)01-0017-09](https://doi.org/10.11883/1001-1455(2005)01-0017-09)
20. Wang L, Li Y, Ma ZH (2022) The radial stiffness calculation and parameter optimization of the annular rubber shock absorber based on Mooney-Rivlin model. *Acta Armamentarii* 43(51):35–45. <https://doi.org/10.12382/bgxb.2022.A008>
21. Wang BZ, Zhou XR, Hu SS (2008) Dynamic mechanical behavior and rate-temperature equivalence of rubber. *Polym Mater Sci Eng* 24(8):5–8. <https://doi.org/10.16865/j.cnki.1000-7555.2008.08.002>
22. Chang XL, Lai JW, Zhang XJ, Hu K, Qi W (2014) High strain-rate viscoelastic constitutive model for HTPB propellant. *J Propuls Technol* 35(01):123–127. <https://doi.org/10.13675/j.cnki.tjjs.2014.01.001>
23. Bai Y, Liu CM, Huang GY, Li W, Feng SS (2016) A hyper-viscoelastic constitutive model for polyurea under uniaxial compressive loading. *Polymers* 8(4):133. <https://doi.org/10.3390/polym8040133>

**Publisher's Note** Springer Nature remains neutral with regard to jurisdictional claims in published maps and institutional affiliations.